Acta Crystallographica Section B
Structural Science, Crystal Engineering and Materials
ISSN 2052-5206

Explanation of the stacking disorder in the β-phase of Pigment Red 170

Jaroslav L. Teteruk, Jürgen Glinnemann, Tatiana E. Gorelik, Anthony Linden and Martin U. Schmidt

Acta Cryst. (2014). B**70**, 296–305

Acta Crystallographica Section B: Structural Science, Crystal Engineering and Materials publishes scientific articles related to the structural science of compounds and materials in the widest sense. Knowledge of the arrangements of atoms, including their temporal variations and dependencies on temperature and pressure, is often the key to understanding physical and chemical phenomena and is crucial for the design of new materials and supramolecular devices. *Acta Crystallographica B* is the forum for the publication of such contributions. Scientific developments based on experimental studies as well as those based on theoretical approaches, including crystal-structure prediction, structure–property relations and the use of databases of crystal structures, are published.

Acta Crystallographica Section B
Structural Science, Crystal Engineering and Materials
ISSN 2052-5206

Explanation of the stacking disorder in the β-phase of Pigment Red 170

Jaroslav L. Teteruk,[a] Jürgen Glinnemann,[a] Tatiana E. Gorelik,[b] Anthony Linden[c] and Martin U. Schmidt[a]*

[a]Institut für Anorganische und Analytische Chemie, Goethe-Universität, Max-von-Laue-Strasse 7, D-60438 Frankfurt am Main, Germany, [b]Institut für Physikalische Chemie, Gutenberg-Universität, Welderweg 11, D-55128 Mainz, Germany, and [c]Department of Chemistry, University of Zurich, Winterthurerstrasse 190, CH-8057 Zurich, Switzerland

Correspondence e-mail: m.schmidt@chemie.uni-frankfurt.de

Received 19 April 2013
Accepted 20 November 2013

Dedicated to Harald Schweitzer on the occasion of his 60th birthday

The β-phase of Pigment Red 170, $C_{26}H_{22}N_4O_4$, which is used industrially for the colouration of plastics, crystallizes in a layer structure with stacking disorder. The disorder is characterized by a lateral translational shift between the layers with a component t_y of either +0.421 or −0.421. Order–disorder (OD) theory is used to derive the possible stacking sequences. Extensive lattice-energy minimizations were carried out on a large set of structural models with different stacking sequences, containing up to 2688 atoms. These calculations were used to determine the actual local structures and to derive the stacking probabilities. It is shown that local structures and energies depend not only on the arrangement of neighbouring layers, but also next-neighbouring layers. Large models with 100 layers were constructed according to the derived stacking probabilities. The diffraction patterns simulated from those models are in good agreement with the experimental single-crystal and powder diffraction patterns. Electron diffraction investigation on a nanocrystalline industrial sample revealed the same disorder. Hence the lattice-energy minimizations are able to explain the disorder and the diffuse scattering.

1. Introduction

A crystal structure can be described by an average model representing a time and space average of the atomic positions. This description, however, becomes insufficient when the deviations from the average model have a significant effect on the properties of the material (Welberry, 2005). Disorder can occur in molecular crystals if two or more energetically similar arrangements or conformations of the molecules exist. Insight into the origin of the disorder can be achieved by lattice-energy calculations. These calculations also give detailed information on the local structure, *i.e.* the preferred local arrangements of molecules and the distortions of the individual molecules caused by the positions and orientations of neighbouring molecules. Lattice-energy calculations have been used to explain various types of disorder, including the rotational disorder of molecular fragments like $C_5(CH_3)_5^-$ rings in $(C_5H_5)Fe(C_5(CH_3)_5)$ (Schmidt, 1995), the orientational disorder of entire molecules, *e.g.* in ice, in SF_6 (Dove & Pawley, 1984; Dove *et al.*, 2002) or in $Si[Si(CH_3)_3]_4$ (Dinnebier *et al.*, 1999), the head-to-tail disorder of molecules, *e.g.* of $(CH_3)_3SnV(CO)_6$ (Englert, 2000), or the stacking disorder in layered structures, as in eniluracil (Price *et al.*, 2008) or in tris(bicyclo[2.1.1]hexeno)benzene (Schmidt & Glinnemann, 2012).

Here we use lattice-energy minimizations to explain the severe stacking disorder in the layer structure of the β-polymorph of Pigment Red 170.

Pigment Red 170 (P.R. 170, see Fig. 1) is an industrially produced organic pigment used for the colouration of lacquers and plastics (Herbst & Hunger, 2004). The pigment is synthesized in water yielding a nanocrystalline α-phase. Heating a suspension of the α-phase in water at $\sim$ 3 bar to 403 K yields the γ-phase (Ribka, 1970). The crystal structures of the α- and γ-phases were determined from X-ray powder diffraction data using the results of lattice-energy minimizations (Schmidt *et al.*, 2006; see Fig. S1 in the supporting information[1]). The α-phase exhibits an ordered herringbone packing in the space group $P2_12_12_1$ (No. 19), Z = 4, with a three-dimensional hydrogen-bond network. The γ-phase forms an ordered structure with wavy layers in $P2_1/n$ (No. 14), Z = 4.

The nanocrystalline β-phase, which is mainly used for the colouration of plastics, is industrially produced by heating an aqueous suspension of the α-phase to 373 K. Single crystals of the β-phase were obtained by recrystallization from *N*-methyl-2-pyrrolidone (NMP) at 473 K. The X-ray single-crystal diffraction pattern of these crystals consists of Bragg reflections and strong diffuse streaks through the Bragg reflections. The diffuse scattering is also evident from X-ray powder diffraction (XRPD) data and electron diffraction (ED) data (see §3.1). Evaluation of only the Bragg reflections in the X-ray single-crystal data leads to the average structure (Warshamanage *et al.*, 2014). Two models were developed, both having a monoclinic unit cell with a = 14.4 Å, b = 24.8 Å, c = 25.0 Å, $\alpha = \gamma = 90°$, $\beta = 109.8°$, V = 8392 Å^3, Z = 16 at 100 K (Fig. S2). In this unit cell, model **1** contains an unconventional glide plane with the glide part of (**a** − **c**)/4, denoted by the general glide symbol *g* (Fischer & Koch, 2011). This yields the space group $B12_1/g1$ (which is an unconventional setting of $P12_1/c1$) with Z' = 2 (Fig. S2*a*). This unconventional setting was chosen in order to describe both models with the same lattice parameters. Model **2** is described in space group $P12_1/a1$ (which is a non-standard setting of $P12_1/c1$) with Z' = 4 (Fig. S2*b*). In both models the molecules are arranged in almost planar layers parallel to (100). The unit cell contains four layers consisting of four molecules each. In model **1** the molecules are distributed over two positions in the layer, with occupancies of $\sim$ 93 and $\sim$ 7%. Model **2**, which gives a slightly worse fit to the data, contains two symmetry-independent types of layers. Every second layer is ordered; the other layers consist of molecules in two different positions with occupancies of $\sim$ 65 and $\sim$ 35%.

The strong diffuse streaks parallel to **a*** show that both models are only approximations. The actual structure exhibits a stacking disorder. The stacking of the layers is neither periodic nor fully random. Apparently the structure exhibits a preferred local ordering, but this local ordering is difficult to extract from the diffraction data.

In the following we use order–disorder (OD) theory to derive the local symmetry and the possible stacking sequences. Lattice-energy minimizations are performed on a variety of structures with different stacking sequences to reveal the actual local structures and the stacking probabilities. In order to explain the diffuse scattering, large structures with up to 100 layers are constructed according to the stacking probabilities; their diffraction patterns are simulated and compared with the experimental diffraction patterns (including the diffuse scattering). Recently, this approach was successfully applied to explain the stacking disorder and the diffuse scattering of tris(bicyclo[2.1.1]hexeno)benzene (Schmidt & Glinnemann, 2012). Additionally, we describe the ED and XRPD investigations.

2. Experimental and theoretical procedures

2.1. Synthesis and crystallization

Sample (I): About 1 ton of P.R. 170 was industrially synthesized by azo-coupling in water with subsequent heating of the pigment suspension with additives in water to 373 K, as described by Ribka (1966; Example 4). The resulting nanocrystalline α-phase was transformed into the β-phase by heating in suspension to 373 K. In order to prove that the crystal structure of the industrially produced material corresponds with that of the single crystals of Sample III, a very small portion of the industrial product was used for electron diffraction without further treatment (samples from Novoperm Red F5RK Lot 47410).

Sample (II): To improve the crystallinity, the synthesis was repeated on a lab scale without any additives; the press-cake of the α-phase was suspended in a mixture of 90% *iso*-butanol and 10% water, and stirred at $\sim$ 4 bar to 413 K for 20 h. The resulting powder of the β-phase was used for X-ray powder diffraction.

Sample (III): Single crystals of the β-phase were obtained by recrystallization from *N*-methyl-2-pyrrolidone (NMP) at $\sim$ 473 K and used for the X-ray single-crystal analysis of the

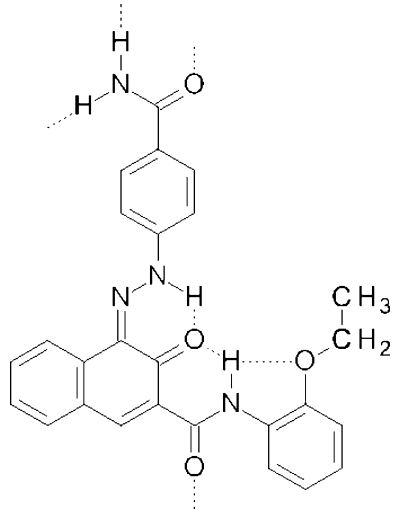

Figure 1
The molecule of P.R. 170, $C_{26}H_{22}N_4O_4$, with intra- and intermolecular hydrogen bonds shown as dotted lines.

[1] Supporting information for this paper is available from the IUCr electronic archives (Reference: OG5063).

average structure, as described in the preceding paper (see Warshamanage *et al.*, 2014).

2.2. Electron microscopy and electron diffraction

Sample (I) was prepared for TEM investigations by suspending the pigment in *n*-hexane using an ultrasonic bath. A drop of the suspension was placed onto a holey carbon-film-coated copper grid and dried under vacuum. TEM investigations were performed with a TECNAI F30 transmission electron microscope equipped with a field emission gun operating at 300 kV. Electron diffraction data were collected using a high-tilt tomography holder (FISCHIONE) within a $\pm 60^\circ$ tilt range with a tilt step of 1°. The diffraction data were recorded on a 1k GATAN CCD camera.

Electron diffraction zonal patterns were collected in nano-diffraction mode using a 10 µm C2 condenser aperture; automated diffraction tomography (ADT) data were collected using the dedicated acquisition module (Kolb *et al.*, 2007). ADT data were processed using the *ADT3D* software (NANOMEGAS, Belgium).

The crystals degraded under electron irradiation. The rate of the degradation was measured using a set of subsequently acquired electron diffraction patterns (Kolb *et al.*, 2010). The characteristic dose of the material was estimated to be 120 $e^- Å^{-2}$ ($1/e$ fall off of total Bragg reflection intensity). Consequently, the TEM work was done using a 3 $e^- Å^{-2} s^{-1}$ dose rate, which allowed 40 s exposure of the material until the $1/e$ decay was reached.

2.3. X-ray powder diffraction

X-ray diffraction was performed in transmission mode on a Stoe Stadi-P diffractometer, equipped with a primary Ge (1 1 1) monochromator and a linear position-sensitive detector. Cu $K\alpha_1$ (λ = 1.5406 Å) radiation was used. The sample was kept in a capillary. The measurements were performed at 100 K in order to be consistent with the single-crystal diffraction experiments of Warshamanage *et al.* (2014).

2.4. Lattice-energy minimizations

2.4.1. Model building. Lattice-energy minimizations were performed on ordered model structures with correspondingly large unit cells. All models were constructed in a reference cell with the starting parameters a = 7.2 Å (or multiples of it), b = 24.8 Å, c = 25.0 Å, $\alpha = \gamma = 90^\circ$ and $\beta = 109.8^\circ$ with the stacking direction **a**. The molecular layers were parallel to the (1 0 0) plane, and contained four molecules per layer unit cell.

The stacking sequences were different for all models. Three approaches were used to set up the model structures:

(*a*) Starting from model **1** and choosing for each layer either the atomic positions with 93% occupancy or the positions with 7% occupancy.

(*b*) Starting from model **2**; the fully occupied layers are taken without modification. For each disordered layer one of the positions with either 65% occupancy or 35% occupancy is chosen.

(*c*) Building the structure layer-by-layer using the local symmetry elements (see §3.2.3). The resulting sequences include not only all models derived by approaches (*a*) and (*b*), but also combinations of (*a*) and (*b*) as well as additional monoclinic and triclinic structures not covered by models **1** and **2**.

2.4.2. Lattice-energy minimizations. The calculations were performed using the program suite *Materials Studio* (Accelrys, 2008), using a Dreiding force-field (Mayo *et al.*, 1990) with tailor-made modifications concerning the intramolecular force-field parameters in order to improve the calculated molecular geometry, especially for the hydrazone group (for details see the supporting information). The van der Waals interactions were calculated not by the usually applied 6-12 potentials, but by the 6-exp potentials recommended by the developers of the force-field (Mayo *et al.*, 1990). Atomic charges were obtained from *ab initio* calculations with the 6-311G** function set (McLean & Chandler, 1980) using the program *GAUSSIAN03* (Frisch *et al.*, 2004), with a subsequent fit to the electrostatic potential (details are given in the supporting information). During the lattice-energy minimizations the lattice parameters were kept fixed to prevent changes in the layer stacking during optimization and to avoid a transition into the more stable γ-phase structure. All atomic positions were optimized and all molecules were treated as flexible throughout. All energies are given in kJ mol^{-1}.

2.4.3. Simulation of diffraction patterns and diffuse scattering. The models obtained and probabilities of the local stacking patterns, derived using the Boltzmann distribution, are used to simulate single-crystal X-ray diffraction patterns using the program suite *Cerius2* (Accelrys, 2003). The diffuse scattering was simulated by calculating single-crystal diffraction patterns of structural models with correspondingly large unit cells (*e.g.* 100 layers). X-ray powder diffraction patterns were calculated with the software *WinXPOW* (Stoe & Cie, 2004).

3. Results and discussion

3.1. Electron microscopy, electron diffraction and X-ray powder diffraction

3.1.1. Electron microscopy and electron diffraction. The industrially produced nanocrystalline powder of β-P.R. 170 [Sample (I)] consists of elongated crystals with a length of 100–200 nm. The crystals all look alike and have a relatively narrow size distribution. Higher magnification images showed that the crystals tend to have a rectangular shape, but rounded edges between the facets (see the supporting information, Fig. S5*a*).

Electron diffraction patterns exhibit sharp reflection spots together with diffuse streaks. Three-dimensional diffraction data reconstructed from ADT data show streaks of diffuse scattering extending along one direction throughout the reciprocal space. In order to remain consistent with the previously defined unit cell, **a*** was assigned parallel to the diffuse scattering direction (Fig. 2).

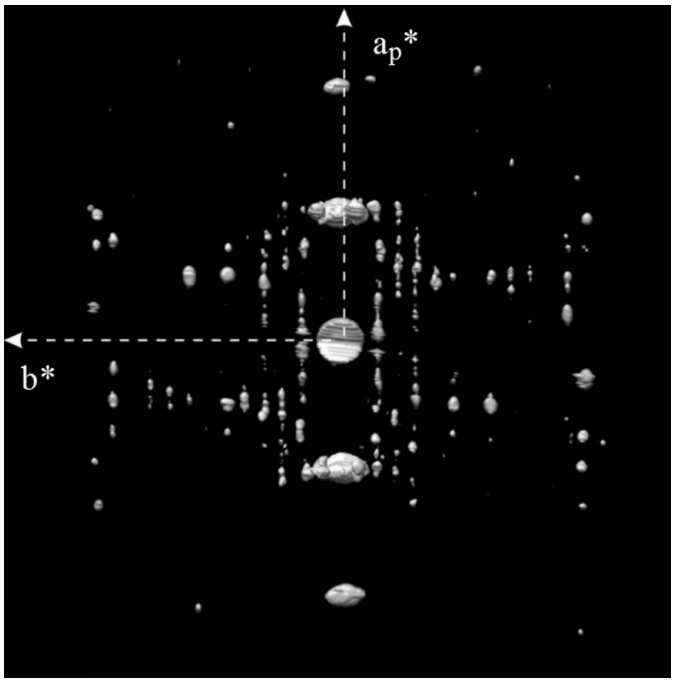

Figure 2
Projection of three-dimensional ED data reconstructed from ADT data. Direction of view **c***.

Most crystals were oriented with the **a** axis more or less parallel to the carbon film, *i.e.* perpendicular to the electron beam. Thus, the diffuse streaks could be directly recorded in the electron diffraction. A projection showing the diffuse streaks is presented in Fig. 2. The four strongest reflections are the 4 0 0, 8 0 0, $\bar{4}$ 0 0 and $\bar{8}$ 0 0 reflections, which correspond to the layer stacking of the molecules. The electron diffraction data show similar features to those observed in the single-crystal X-ray analysis. This proves that the stacking disorder is present not only in the single crystals grown from solvents, but also in the industrial product used for the colouration of plastics.

3.1.2. X-ray powder diffraction. The experimental X-ray powder diffraction patterns of the nanocrystalline industrial product [Sample (I)] and of the powder sample with improved crystallinity [Sample (II)] correspond to the powder diffraction pattern calculated directly from the raw single-crystal diffraction data of the recrystallized sample (III) (see the supporting information). Temperature-dependent X-ray powder diffraction confirmed that the β-phase does not undergo a phase transition between room temperature and 100 K (the temperature of the X-ray single-crystal analysis by Warshamanage *et al.*, 2014).

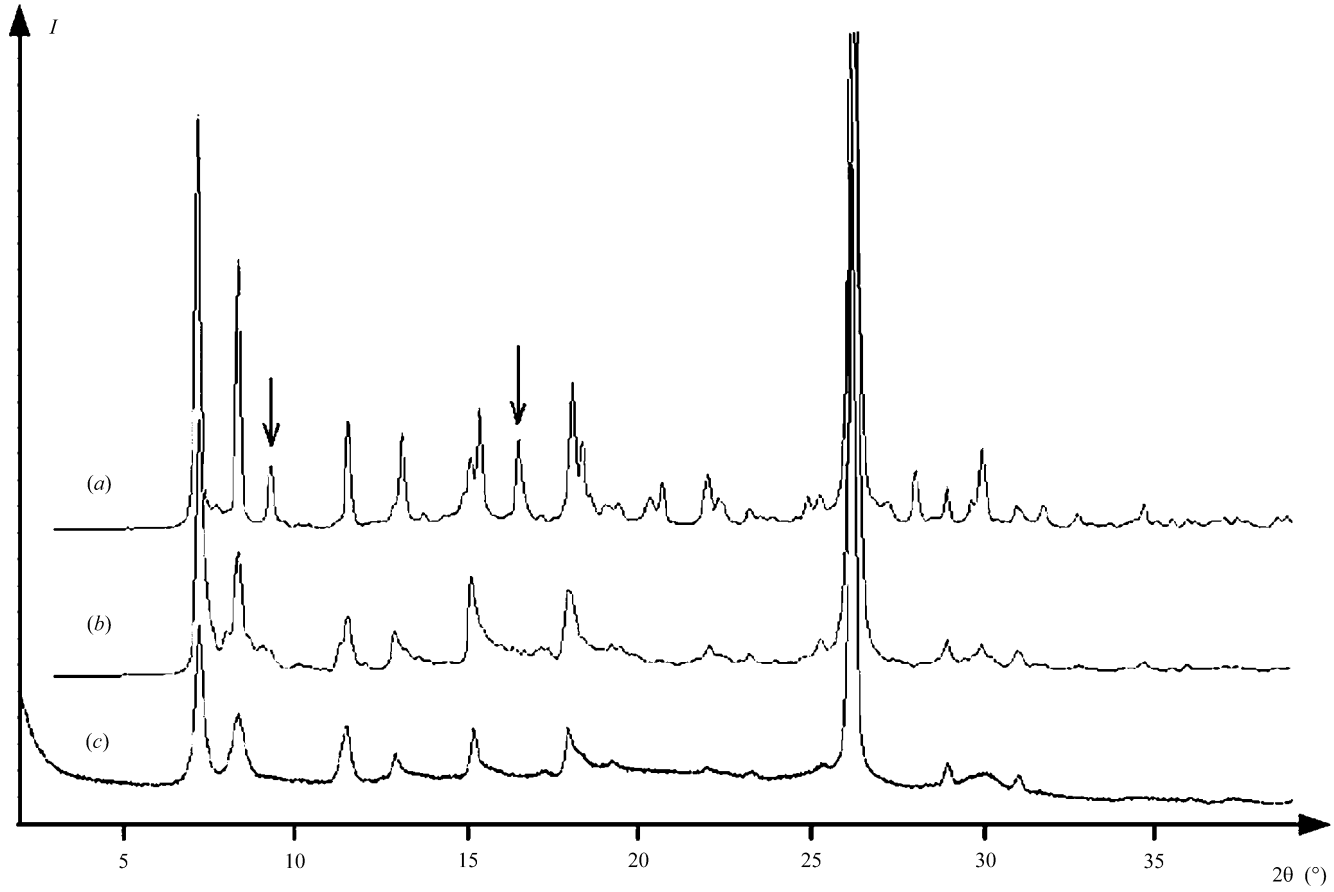

Figure 3
X-ray powder diffraction patterns (λ = 1.5406 Å). For details see §3.4. From top to bottom: (*a*) simulated pattern from a hundred-layer structure with a fully random sequence; (*b*) simulated pattern from a hundred-layer structure constructed according to local structure; (*c*) experimental diffraction pattern, recorded at 100 K. The arrows in (*a*) denote reflections absent in the experimental pattern.

The powder pattern of the β-phase shows nine relatively sharp and six broad reflections (Fig. 3*c*). The strong sharp reflection at $2\theta = 26.2^\circ$ corresponds to $d = 3.4$ Å which is typical for the layer stacking distance of aromatic compounds and is in good agreement with the value of 1.7 Å for the van der Waals radius of carbon. The reflections at $2\theta = 12.9^\circ$, $2\theta = 15.2^\circ$ and $2\theta = 17.9^\circ$ show a strange shape with an unusual tail to higher diffraction angles. Such reflection profiles are typically due to diffuse scattering caused by short-range order (Warren, 1969). These reflection profiles could be explained by lattice-energy minimizations.

3.2. Order–disorder (OD) theory

In the β-phase of P.R. 170 different stacking sequences of equivalent layers should be described as a case of polytypism. Adjacent layers in this structure can be connected by equivalent symmetry operations described in §§3.2.2 and 3.2.3, which permit ordered and disordered infinite layer sequences. The whole set of stacking sequences is called a family of OD structures (Dornberger-Schiff & Fichtner, 1972). A recent account of the OD theory of polytypic structures is given by Ferraris *et al.* (2008).

3.2.1. Layer symmetry. A single layer can be described with a unit cell with lattice parameters of $b = 24.755$ Å, $c = 24.974$ Å, $\alpha = 90^\circ$. This unit-cell contains four molecules, which are connected by hydrogen bonds. The layer is almost, but not exactly, planar.

Within the layer the molecules are symmetry-related by inversion centres, 2_1 screw axes parallel to **b** and *c*-glide planes perpendicular to **b** (Fig. 4). Thus, the layer group symbol is $p12_1/c1$, which is a non-standard setting of $p2_1/b11$ (No. 17) (Kopský & Litvin, 2002). If the layers were exactly planar, the layer group would be $p2/m2_1/c2_1/b$, a non-standard setting of $p2_1/b2_1/a2/m$ (No. 44), and the plane group would be $p2gg$. Layers with the same hydrogen-bond pattern, but stronger deviations from planarity, are found in the γ-phase ($b = 24.17$ Å, $c = 25.43$ Å, $\alpha = 90^\circ$).

3.2.2. Layer arrangement. The layers are stacked along **a**. The next layer is generated from the first layer by translation along the vector $(\frac{1}{4}, t_y, \frac{1}{4})$ (referring to the lattice parameters of the average structure models) with $t_y = +0.421$ or -0.421. The $(\frac{1}{4}, +0.421, \frac{1}{4})$ vector is denoted in the following as '**+**', while the $(\frac{1}{4}, -0.421, \frac{1}{4})$ vector is denoted as '**–**', see Fig. 4. In the following we will denote all stacking sequences by their translational shift vectors.

If the layers were exactly planar, there would be two further possibilities for stacking a second layer on top of a given one. Apart from the vectors '**+**' and '**–**' with a translational component in the **+c** direction, the shift could occur in the **−c** direction, leading to vectors '**p**' and '**q**', see Fig. 4.

If only two layers are considered, and the layers were exactly planar, the four arrangements '**+**', '**–**', '**p**' and '**q**' would have the same energy. However, the packing becomes more efficient when the layers deviate from planarity. Due to this distortion, the vectors '**p**' and '**q**' become inequivalent to the vectors '**+**' and '**–**'. Structures containing only the vectors '**+**' and '**–**' are energetically as favourable as the corresponding structures containing only the vectors '**p**' and '**q**', but a transition from '**+**' and '**–**' to '**p**' and '**q**' costs more than 8 kJ mol^{-1}, as revealed by test calculations, *e.g.* of the sequences '**+ + – – p p q q**' *versus* '**+ + – – + + – –**'. Hence the vectors '**p**' and '**q**' could be disregarded. They are also not observed experimentally.

The experimental model **1**, derived from single-crystal data, would permit that the molecules on two subsequent layers are all situated at the minor occupied positions (*cf.* Fig. 7*a*; positions denoted as '1'). This would result in an interlayer shift of $t_y = 3 \times 0.421 = 1.263$, which is inconsistent with the stacking rule of $t_y = \pm 0.421$. This arrangement is energetically very unfavourable (see the supporting information). Hence the sequences containing '...11...' fragments will be disregarded.

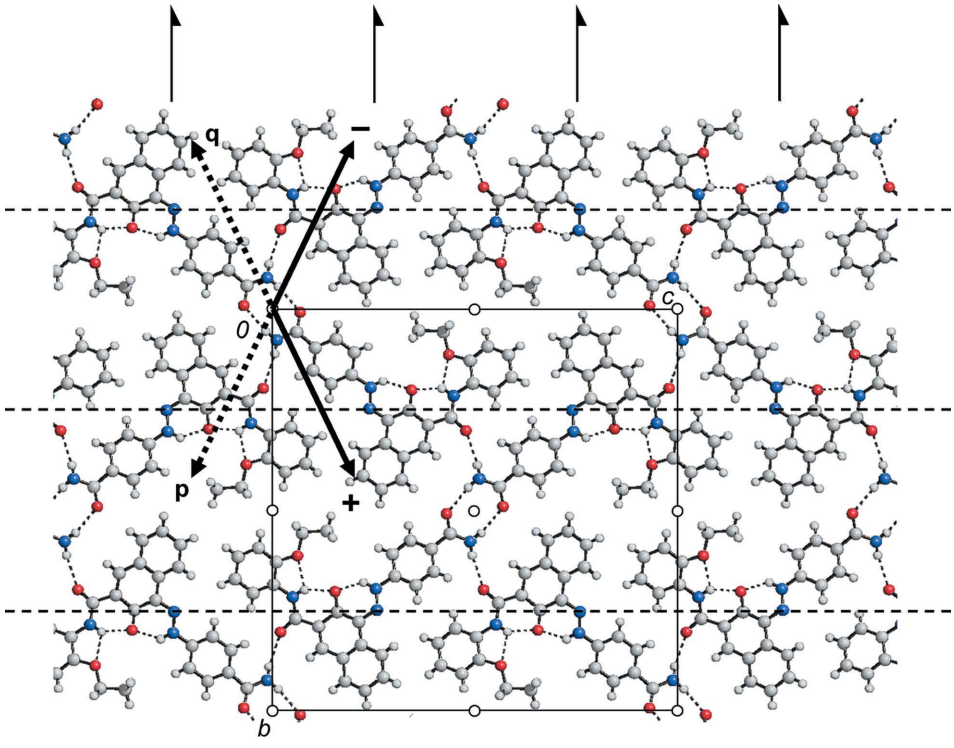

Figure 4
An individual layer and its symmetry elements viewed perpendicular to the layer. The vectors '**+**' and '**–**' represent the possible translational shift vectors to a subsequent layer. For an explanation of vectors '**p**' and '**q**' see §3.2.2.

The exclusive consideration of the translation vectors '**+**' and '**–**' permits an easy application of the order–disorder (OD) theory.

3.2.3. Symmetry elements between neighbouring layers. The combination of the translation vector $(\frac{1}{4}, \pm 0.421, \frac{1}{4})$ with the symmetry elements of the layer group $p12_1/c1$ results in three additional symmetry elements (see Figs. 5 and 6).

(1) A combination of translation and inversion generates inversion centres between the layers.

(2) A combination of translation and *c*-glide planes results in *g*-glide planes perpendicular to **b** with a glide vector $+\frac{1}{4}(\mathbf{a} - \mathbf{c})$. Since the layer thickness in **a** direction is $\mathbf{a}_0 = \mathbf{a}/4$, the glide vector equals $\mathbf{a}_0 - \frac{1}{4}\mathbf{c}$.

(3) A combination of translation with the 2_1 axes within the layer yields twofold screw axes parallel to **b** with a fractional screw vector of $\pm 0.079\mathbf{b}$.

If the t_y component in the **b** direction was $t_y = 0.50$ instead of ± 0.421, the local screw axes would become global twofold axes, the structure would be ordered, and would have the space group $C12/c1$ with $Z = 8$, $Z' = 1$, with all molecules being symmetry-equivalent. Yet the translational component is ± 0.421; consequently, not all local symmetry elements can be incorporated into the crystallographic symmetry; the others remain as local symmetry elements. This holds for all stacking sequences.

In the notation of the OD theory, any glide plane is denoted as $n_{r,s}$. For glide planes perpendicular to **b** and with $\mathbf{a}_0$ as the non-translational vector, the translational component equals $s\frac{\mathbf{a}_0}{2} + r\frac{\mathbf{c}}{2}$. For the present *g*-glide plane this results in the symbol $n_{-1/2,2}$. A twofold screw axis parallel to **b** may be denoted as 2_t with a screw vector of $t\frac{\mathbf{b}}{2}$. For the present twofold screw axes this results in the symbol $2_{\pm 0.158}$.

The OD groupoid family symbol gives the layer symmetry in the first line and the interlayer symmetry operations in the following one or two lines. The stacking direction is denoted as (1) (Dornberger-Schiff, 1956). Consequently, the groupoid family symbol of the β-phase of P.R. 170 is

$$P \quad \begin{matrix} (1) & \frac{2_1}{c} & 1 \\ \{(1) & \frac{2_{\pm 0.158}}{n_{-1/2,2}} & 1\}. \end{matrix}$$

3.2.4. Stacking and stacking disorder. Repeated application of the '+' shift results in a triclinic structure with sequence '+ + + +' with lattice parameters of a = 6.373 Å, b = 24.755 Å, c = 24.974 Å, $\alpha = 90°$ (fixed due to the layer symmetry), $\beta = 37.965°$ and $\gamma = 107.944°$, in the space group $P\bar{1}$, Z = 4, Z' = 2. This structure is not

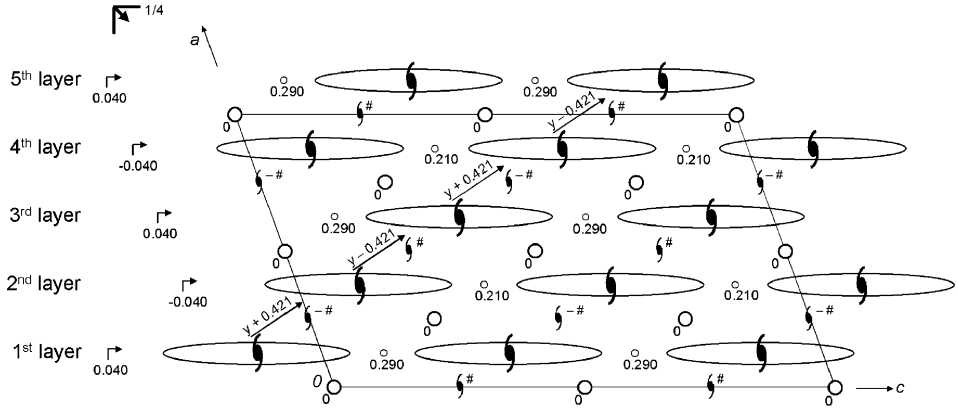

Figure 5
Local and global symmetry elements in the stacking sequence '+ − + −', which corresponds to the major occupied positions in model **1**. Direction of view [0 1 0]. Molecules are sketched as ellipses. The space group is $B2_1/g$. The numbers denote the y coordinates of the symmetry elements. The diagonal glide plane at $y = \frac{1}{4}$ is a *g*-glide plane with a translational vector of $(\frac{1}{4}, 0, -\frac{1}{4})$. The B-centring, the inversion centres at $y = 0$, the diagonal *g*-glide planes at $\frac{1}{4}$ and $\frac{3}{4}$, and the screw axes within the layers are global symmetry elements. All other symmetry elements are local symmetry elements.

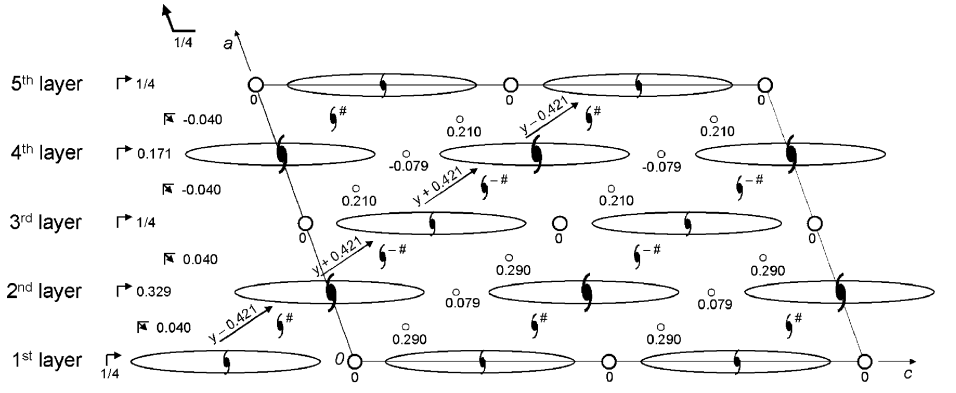

Figure 6
Local and global symmetry elements in the stacking sequence '− + + −', which corresponds to the full and major occupied positions in model 2. Direction of view [0 1 0]. Molecules are sketched as ellipses. The space group is $P2_1/a$. The numbers denote the y coordinates of the symmetry elements. The diagonal glide planes at $y = 0.040$ and $y = -0.040$ are *g*-glide planes with a translational component of $(\frac{1}{4}, 0, -\frac{1}{4})$. The inversion centres in the first, third and fifth layer, the screw axes in the second and fourth layer and the *a*-glide planes at $\frac{1}{4}$ and $\frac{3}{4}$ are global symmetry elements. All other symmetry elements are local symmetry elements.

observed experimentally, neither in the hundreds of recorded powder diagrams of different samples of P.R. 170, nor as a domain in the single-crystal diffraction patterns.

Repeated application of the *g*-glide planes results in the periodic sequence '+ − + −', which corresponds to the major occupied molecular positions of model **1** (Fig. 7*a*) and to the sequence 'full – 0.35 – full – 0.65' occupied positions in model **2** (Fig. 7*b*). This sequence can be described in space group $B12_1/g1$, $Z = 16$, $Z' = 2$, which is a non-standard setting of $P2_1/c$. Both structures '+ + + +' and '+ − + −' have a maximum degree of order (MDO; Dornberger-Schiff, 1982).

The sequence '− + + − − + + −' (Fig. 7, right) can be described in space group $P2_1/a$, $Z = 16$, $Z' = 4$, and corresponds to model **2**, if only the full (1.00) and major (0.65) occupied positions are selected. This sequence is not a MDO structure since it requires at least two different symmetry operations.

Sequences with a higher number of repeating '+' or repeating '−' shifts are theoretically possible, *e.g.* '+ + + + − − − −'. They lead to positions which are shifted by multiples of ±0.421 against the starting positions. These additional positions are marked by 'W', 'X' and 'Y' in Fig. 7. Positions X and Y were observed experimentally with very low occupancies. Shadows in the difference Fourier map for model 1 might be indicative of the existence of low-occupancy sites at position W, but this could not be confirmed or excluded conclusively, even during the subgroup analysis carried out by Warshamanage *et al.* (2014).

Note that all these periodic structures are only approximate models of the actual structure. Actually, the crystal is built by a non-periodic sequence of '+' and '−' translations.

The preferred local arrangements are calculated by means of lattice-energy minimizations.

3.3. Lattice-energy minimizations

3.3.1. Single layer. A lattice-energy minimization of a single layer *in vacuo* results in the tilting of molecules against the layer plane, similar to what is seen for the α- and γ-phases. The pattern of hydrogen bonds remains unchanged. This shows that the experimentally and theoretically observed planar layer geometry is a result of packing effects, *i.e.* of the interactions with the neighbouring layers.

3.3.2. Preferred stacking sequences. Lattice-energy minimizations were made with periodic models containing up to 12 layers (Table 1).

All models can be set up in different ways, *e.g.* '+ +' is symmetry-equivalent to '− −', and '− + + −' is symmetry-equivalent to '+ + − −', '+ − − +' and '− − + +'. Correspondingly, the model '+ +' has a degeneracy $g_i = 2$, and the model '− + + −' has $g_i = 4$ *etc*.

Within the 4-layer models the sequence '− + + −' is energetically the best one. The reason might be sought in the fine details of the layer geometry and in long-range Coulomb and van der Waals interactions between next-neighbouring layers. It is this '− + + −' sequence which is formed by the experimental model 2, if only the major occupied positions (or only the minor occupied positions) are chosen in addition to the fully occupied positions. The '− + + −' structure is still the most favourable one among all 8-layer models, but not among the 12-layer models. Interestingly, the best energy of the 12-layer models is not found for one of the simple stacking motifs,

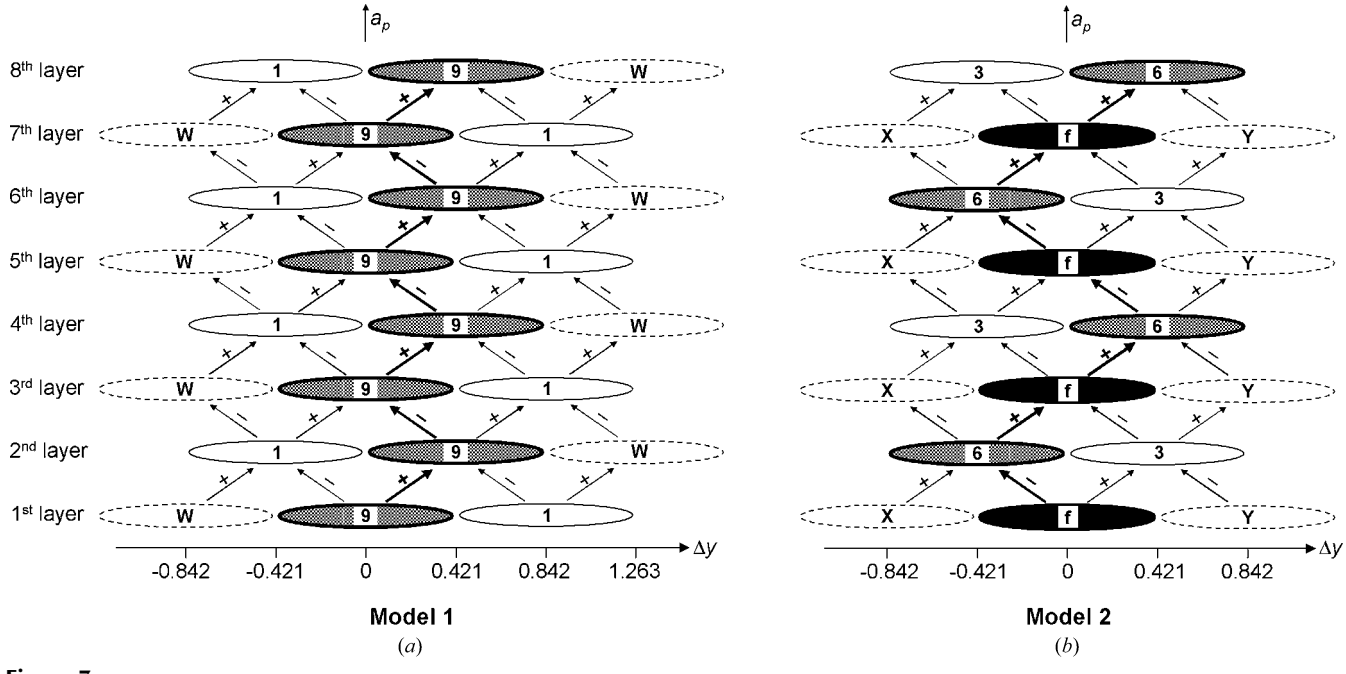

Figure 7
Lateral positions of the molecules in (*a*) model **1** and (*b*) model **2**. Direction of view [0 0 1]. Only molecules related by translation are drawn. '**+**' and '**−**' denote a shift by $t_y = +0.421$ and -0.421, respectively. Symbols f, 9, 6, 3 and 1 denote the experimentally determined occupancies of 1.00 (full), 0.93, 0.65, 0.35 and 0.07, respectively. Symbols W, X and Y denote additional positions. For example, the periodic sequence '9199' corresponds to 'f6f6' and '**− + + −**'.

Table 1
Results of the lattice-energy minimizations.

Energies are given in kJ mol^{-1} relative to the '+ +' sequence. For the notation of the sequences see the text. g_i denotes the degeneracy (*i.e.* the number of symmetry-equivalent possibilities of each model for a given number of layers).

Stacking sequence	Sequence in model 1	Sequence in model 2	Symmetry of the model	Degeneracy g_i	Relative energy (kJ mol^{-1})
2-layer models (Z = 8)					
+ +			$P\bar{1}$, Z = 4	2	0
+ −	99		$P2_1/n$, Z = 8	2	−1.17
			Degeneracy sum:	4	
4-layer models (Z = 16)					
+ + + +			$P\bar{1}$, Z = 4	2	0
+ + + −			$P\bar{1}$, Z = 16	8	−1.53
+ − + −	9999	f3f6	$P2_1/n$, Z = 8	2	−1.17
− + + −	9199	f6f6	$P2_1/a$, Z = 16	4	−2.05
			Degeneracy sum:	16	
6-layer models (Z = 24)					
+ + + + + +			$P\bar{1}$, Z = 4	2	0
+ + + + + −			$P\bar{1}$, Z = 24	12	−1.21
+ + + + − −			$P\bar{1}$, Z = 24	12	−1.42
+ + + − + −			$P\bar{1}$, Z = 24	12	−1.42
+ + − + + −			$P\bar{1}$, Z = 12	12	−1.46
+ − + − + −	999999		$P2_1/n$, Z = 8	2	−1.17
− + − + + −	919199		$P2_1$, Z = 24	6	−1.65
− + + + − −	919919		$P2_1/a$, Z = 24	6	−1.30
			Degeneracy sum:	64	
Selected 8-layer models (Z = 32)					
+ + + + + + + +			$P\bar{1}$, Z = 4	2	0
+ + + + + + + −			$P\bar{1}$, Z = 32	16	−0.99
+ + + + + + − −			$P\bar{1}$, Z = 32	16	−1.23
+ − + − + − + −	99999999	f3f6f3f6	$P2_1/n$, Z = 8	2	−1.17
− + + − − + + −	91999199	f6f6f6f6	$P2_1/a$, Z = 16	4	−2.05
+ + + + − − − −	W1991991	x6f6y3f3	$P2_1/a$, Z = 32	8	−1.41
Selected 10-layer models (Z = 40)					
+ + + + + + + + + +			$P\bar{1}$, Z = 4	2	0
+ − + − + − + − + −	9999999999		$P2_1/n$, Z = 8	2	−1.17
− + + − + − + − + −	9199999999		$P2_1$, Z = 40	10	−1.80
Selected 12-layer models (Z = 48)					
+ + + + + + + + + + + +			$P\bar{1}$, Z = 4	2	0
+ + + + + + + + + + + −			$P\bar{1}$, Z = 48	24	−0.73
+ − + − + − + − + − + −	999999999999	f3f6f3f6f3f6	$P2_1/n$, Z = 8	2	−1.17
− + + − − + + − − + + −	919991999199	f6f6f6f6f6f6	$P2_1/a$, Z = 16	4	−2.05
+ − + − + − + + − + − −	999999991919	f3f6f3f6Y3Y6	$P2_1$, Z = 48	24	−2.09
+ − + − + − + − + + − −	999999999919	f3f6f3f6f3Y6	$P2_1$, Z = 48	24	−1.71

but for a structure with the quite irregular sequence '+ − + − + − + + − + − −', which is by the insignificant amount of 0.04 kJ mol^{-1} more favourable than the sequence '− + + −'. Comparable energies are also found in other sequences containing a mixture of '+ −' and '− + + −' motifs. These sequences differ from each other in energy by less than 0.5 kJ mol^{-1}; except that the pure '+ −' sequence is $\sim$0.87 kJ mol^{-1} less favourable than the pure '− + + −' sequence. The high number of energetically similar structures causes the disorder, which is experimentally observed as diffuse streaks.

3.3.3. Influence of neighbouring and next-neighbouring layers. The hydrogen-bond topology and the overall arrangement of molecules is identical in all layers. The geometry of a given layer depends slightly on the position of neighbouring and next-neighbouring layers. For example, the atomic positions of the central layer in the sequences 9**9**9 and 1**9**9 differ from each other by an r.m.s. value of only 0.157 Å; the largest difference is 0.32 Å. The influence of the next-neighbouring layer is also not negligible: the atomic positions of the central layer in 99**9**99 and 19**9**91 differ only by 0.128 Å (r.m.s.d.), with a maximum deviation of 0.28 Å. The layers interact through van der Waals and Coulombic interactions. The interactions between next-neighbouring layers consist of two parts: (*a*) conveyed by the neighbouring layer; (*b*) direct through-space van der Waals and Coulombic interactions. Both parts vary by $\sim$1 kJ mol^{-1} depending on the sequence (see the supporting information for details).

The fact that all layers have a similar geometry is proven by the single-crystal data: larger deviations of the atomic positions would lead to split atoms or strongly anisotropic displacement parameters (ADPs) in the average structure. However, these features are absent in the average structure models of β-P.R. 170.

3.3.4. Local stacking probabilities. From the energies of the periodic models, given in Table 1, one can calculate the probability of finding a specific stacking pattern in a non-periodic infinite stacking (*e.g.* four subsequent layers in a '...+ + −...' stacking pattern; for details see the supporting information). For 4-layer patterns, these probabilities are 15% for '...+ + +...' or '...− − −...', 23% for '...− + −...' or '...+ − +...' and 62% for the remaining patterns ('...+ + −...', '...− − +...', '...+ − −...' or '...− + +...'). These probabilities can be used for building large structural models with *e.g.* 100 layers (see next section).

3.4. Large sequences; simulation of the diffuse scattering

Diffraction patterns for disordered structures can successfully be simulated from models with large supercells. For this purpose medium-sized structures with up to 10 layers (2240 atoms) were fully optimized. Larger structures were then constructed by overlapping pre-optimized fragments. The molecular geometry was either taken from the lattice-energy calculation results or from the X-ray data; both approaches resulted in visually identical diffraction patterns.

Figs. 8(*a*) and 9(*a*) show simulated single-crystal diffraction patterns of a model containing 100 layers with a purely random layer sequence. Comparison with experimental diffraction patterns (Figs. 8*c* and 9*c*) reveals that this model of a fully statistical disorder does not account for the observed

diffraction patterns. Obviously, a purely random stacking is not an appropriate model for the stacking disorder.

As an improved representation of the β-phase of P.R. 170, a new hundred-layer model was constructed according to the calculated local structure, including deviations from the average structure and the derived stacking probabilities.. This model yields the diffraction patterns given in Figs. 8(*b*) and 9(*b*). They show a vastly improved agreement with the experimental single-crystal diffraction patterns. While all patterns show strong diffuse streaks parallel to the **a*** axis, the approach with models that take the local structure into account reproduces further features of the experimental diffraction patterns.

Similarly, the experimental X-ray powder diffraction pattern is not very well reproduced by the hundred-layer model with a random stacking sequence. The simulated powder pattern shows notable additional reflections at ~ 9.5 and $\sim 16.5^\circ$ in 2θ, as indicated by arrows in Fig. 3(*a*), and does not reproduce reflection profiles well.

The improved model built according to the local stacking probabilities yields much better results (Fig. 3*b*). The simulations even reproduce the anomalous reflection profiles with tails to higher 2θ angles, which are caused by the diffuse scattering.

Hence, even for the simulation of powder diffraction patterns, the local structure must be taken into account.

4. Conclusion

The structure of the β-phase of P.R. 170 consists of ordered layers. Subsequent layers are shifted against each other by ($\frac{1}{4}$,

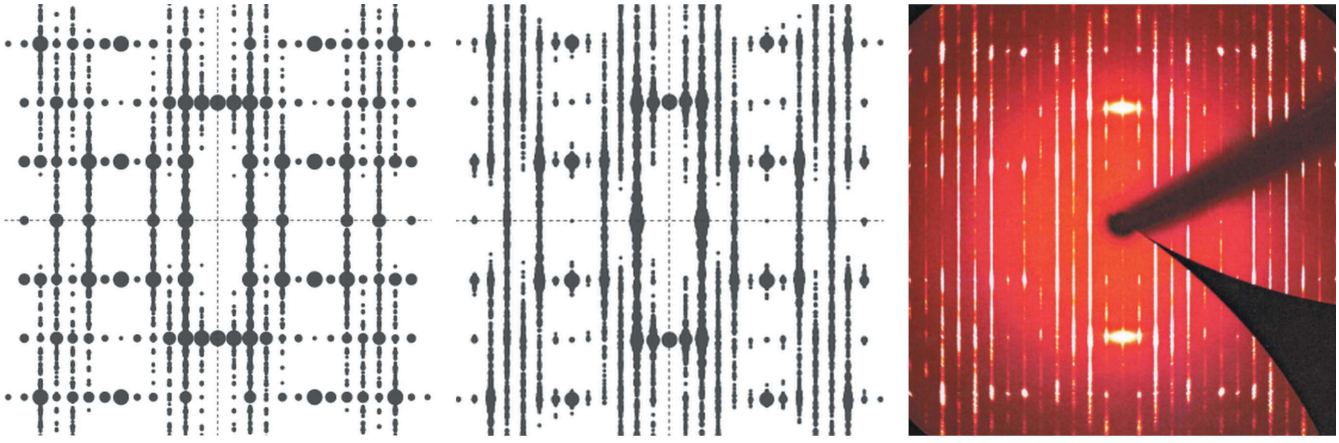

(*a*) (*b*) (*c*)

Figure 8
Simulated and experimental single-crystal diffraction patterns. Zone axis [001]. Reciprocal-lattice layer $hk0$, $h00$ vertical, $0k0$ horizontal. In the simulated patterns, the intensity is represented by the size of the circles. (*a*) Simulated pattern from a hundred-layer structure with fully randomized stacking; (*b*) simulated pattern from a hundred-layer structure featuring the determined local stacking probabilities; (*c*) experimental diffraction pattern.

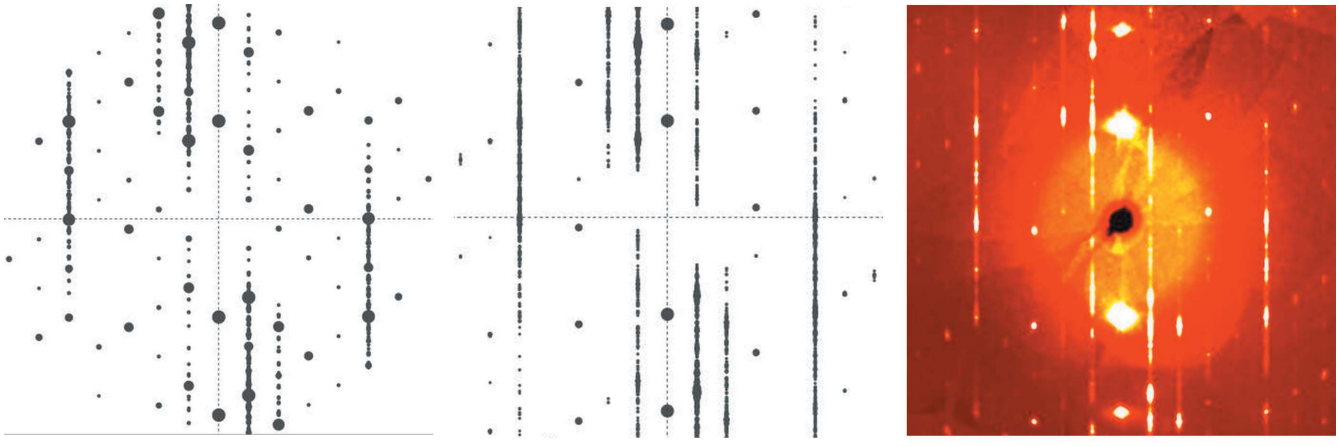

(*a*) (*b*) (*c*)

Figure 9
Simulated and experimental single-crystal diffraction patterns. Zone axis [012], $h00$ vertical. In the simulated patterns, the intensity is represented by the size of the circles. (*a*) Simulated pattern from a hundred-layer structure with fully randomized stacking; (*b*) simulated pattern from a hundred-layer structure featuring the determined local stacking probabilities; (*c*) experimental diffraction pattern.

t_y, $\frac{1}{4}$) with $t_y = +0.421$ or $t_y = -0.421$. The sequence of these stacking vectors is neither periodic nor purely random. The electron diffraction patterns show that this disorder is also present in the nanocrystalline industrial product.

Numerous lattice-energy minimizations were performed on ordered models using a customized force field. Lattice energies obtained by this method show that the structure exhibits a local ordering with preferred sequences. The arrangements of neighbouring and next-neighbouring layers influence the energy and the geometry of the layers.

Local stacking probabilities were calculated by Boltzmann statistics. Using these probabilities, long stacking sequences were constructed, resulting in large supercell models. These models are used for simulations of diffraction patterns, which reproduce the experimental single-crystal X-ray diffraction patterns well, including the diffuse scattering. Also the experimental powder diffraction pattern was reproduced well.

Hence, the lattice-energy minimizations explain the stacking disorder and the diffuse scattering in the β-phase of P.R. 170.

The first inquiry to determine the crystal structure of the β-phase of P.R. 170 was posed to one of the authors (M. U. Schmidt) by Walter Deucker and Hans-Joachim Metz from Hoechst AG in 1994. Syntheses and crystallizations were done by Frank Becker and Tina Simon (both from Clariant GmbH, Frankfurt am Main), Sándor Bekö and Max Hützler (both from Goethe University, Frankfurt am Main). Preliminary electron diffraction investigations were carried out in 2000 by Hans Klee (Clariant GmbH, Frankfurt) and later by Gerhard Miehe (Technical University Darmstadt). The first single-crystal X-ray diffraction experiments, using a laboratory diffractometer with rotating anode and CCD detector, were done in 1999 by Harald Schweitzer and Winfried Heyse (Hoechst Marion Roussel, Frankfurt am Main). Lattice-energy minimizations were partly performed by Christian Czech, Felix Schweighöfer and Ömer Yildiz (all from Goethe-University, Frankfurt). We thank Hans-Beat Bürgi (University of Bern) for cooperation and discussions.

References

Accelrys (2003). *Cerius*^{2}. Accelrys Ltd, Cambridge, England.
Accelrys (2008). *Materials Studio Release Notes.* Accelrys Software Inc., San Diego, USA.
Dinnebier, R. E., Dollase, W. A., Helluy, X., Kümmerlen, J., Sebald, A., Schmidt, M. U., Pagola, S., Stephens, P. W. & van Smaalen, S. (1999). *Acta Cryst.* B**55**, 1014–1029.
Dornberger-Schiff, K. (1956). *Acta Cryst.* **9**, 593–601.
Dornberger-Schiff, K. (1982). *Acta Cryst.* A**38**, 483–491.
Dornberger-Schiff, K. & Fichtner, K. (1972). *Krist. Tech.* **7**, 1035–1056.
Dove, M. T. & Pawley, G. S. (1984). *J. Phys. C Solid State Phys.* **17**, 6581–6599.
Dove, M. T., Tucker, M. G. & Keen, D. A. (2002). *Eur. J. Mineral.* **14**, 331–348.
Englert, U. (2000). *Adv. Mol. Struct. Res.* **6**, 49–74.
Ferraris, G., Makovicky, E. & Merlino, S. (2008). *Crystallography of Modular Materials*, pp. 127–206. Oxford University Press.
Fischer, W. & Koch, E. (2011). *International Tables for Crystallography*, Vol. A, *Space-Group Symmetry*, pp. 810–811. Chester: International Union of Crystallography.
Frisch, M. J. *et al.* (2004). *GAUSSIAN03*, Revision B.01. Gaussian Inc., Wallingford, CT, USA.
Herbst, W. & Hunger, K. (2004). *Industrial Organic Pigments*, pp. 284–287. Weinheim: Wiley-VCH.
Kolb, U., Gorelik, T., Kübel, C., Otten, M. T. & Hubert, D. (2007). *Ultramicroscopy*, **107**, 507–513.
Kolb, U., Gorelik, T. E., Mugnaioli, E. & Stewart, A. (2010). *Polymer Rev.* **50**, 385–409.
Kopský, V. & Litvin, D. B. (2002). *International Tables for Crystallography*, Vol. E, pp. 256–310. Dordrecht, The Netherlands: Kluwer Academic Publishers.
Mayo, S. L., Olafson, B. D. & Goddard III, W. A. (1990). *J. Phys. Chem.* **94**, 8897–8909.
McLean, A. D. & Chandler, G. S. (1980). *J. Chem. Phys.* **72**, 5639–5648.
Price, S. L., Copley, R. C. B., Barnett, S. A., Karamertzanis, P. G., Harris, K. D. M., Kariuki, B. M., Xu, M., Nickels, E. A. & Lancaster, R. W. (2008). *Cryst. Growth Des.* **8**, 3474–3481.
Ribka, J. (1966). German Patent DE 1228731.
Ribka, J. (1970). German Patent DE 2043482.
Schmidt, M. U. (1995). Dissertation. RWTH Aachen, Germany.
Schmidt, M. U. & Glinnemann, J. (2012). *Z. Kristallogr.* **227**, 805–817.
Schmidt, M. U., Hofmann, D. W. M., Buchsbaum, C. & Metz, H. J. (2006). *Angew. Chem. Int. Ed.* **45**, 1313–1317.
Stoe & Cie (2004). *Stoe Win XPOW.* Stoe & Cie GmbH, Darmstadt, Germany.
Warren, B. E. (1969). *X-ray Diffraction*, pp. 227–245. New York: Dover Publications, Inc.
Warshamanage, R., Bürgi, H.-B, Schmidt, M. U. & Linden, A. (2014). *Acta Cryst.* B**70**, 283–295.
Welberry, T. R. (2005). *Z. Kristallogr.* **220**, 993.